Int. J. Electrochem. Sci., 17 **(2022)** Article Number: 220442, doi: 10.20964/2022.04.41

International Journal of
ELECTROCHEMICAL
SCIENCE
www.electrochemsci.org

Short Communication

Micro-electrical discharge machining of Titanium alloy (Ti-6Al-4V) by Sawtooth pulse current

K. Kalaiarasi[1,*], *C. Senthilkumar*[1], *M. Balamurugan*[2], *R. ArokiaDass*[3]

[1] Department of Mechanical Engineering, University College of Engineering Panruti,
[2] Department of Electronics and communication, University College of Engineering Villupuram
[3] Department of Mechanical Engineering, St.Annes college of Engineering and Technology Panruti
[*]E-mail: kalaiconfident@gmail.com

Received: 26 December 2021 / *Accepted:* 5 February 2022 / *Published:* 4 March 2022

Titanium alloy is an important material that has numerous applications in aerospace, microelectronics, pressure sensor, and biomedical industries. The thermomechanical properties of the Titanium alloy are distinctive which enables using this material in several designing fields. Producing micro holes in a Titanium alloy (Ti-6Al-4V) is a challenging task in traditional machining. To overcome these difficulties in machining Titanium alloys, Electric Discharge Machining (EDM) is appropriate with a right choice of machining parameters for a better machining rate and accuracy. This study aims to investigate the impact of input variables such as current, pulse on time (T_{ON}) with Sawtooth waveform and pulse off time (T_{OFF}) on the machining characteristics of a Titanium alloy in micro-EDM process. Outcomes were measured using reaction surface technique and a face-focused imperative composite rotatable layout. Statistical analysis had been advanced the usage of more than one regression to set up the connection among numerous technique parameters and micro-EDM efficiency process. The significant variables determined the usage of evaluation of variance. Different surface analysis was performed using a scanning electron microscope (SEM) and one of the best machined micro hole was achieved through micro-EDM process.

Keywords: Micro Electric Discharge Machining; Ti-6Al-4V; Response Surface Methodology; Material Removal Rate; Overcut

1. INTRODUCTION

Electric Discharge Machining (EDM) is one of the oldest non-conventional machining processes that continues to be widely used and applied in modern industries as a cutting-edge manufacturing process for handling complex materials [1]. In the process of EDM, material removal occurs as a result of intense and continuous electrical discharges between a tool and the workpiece immersed in an appropriate electrolyte solution. A high stream of electromagnetic energy is created, which leads to the formation of flux under specific conditions such as voltage and gaps between the electrode and the

workpiece with power density in the range of 1000-1020W/m^2. Intense heat (6000–12,000 °C) arises due to increase in the electrostatic power density. Subsequently, melting and removal of the material takes place [2,3]. EDM has been effectively used for complicated dimensions and geometries. EDM is a non-touch machining approach as there is no connection between the device and the workpiece, which ensures that dynamic loading pressure is not created and hardens the machined surface. EDM is widely used in the manufacturing of dies and cutting equipment in aircraft industry and also in the production of surgical instruments because of its intrinsic benefits over other manufacturing methods and its capacity to work with any electrically conductive substance irrespective of its material characteristics [4].

Currently, micro-EDM is the most used approach in the industry for a better machining efficiency for an extensive variety of conductive substances such as ceramic and metallurgic composites [5]. Since micro-EDM can create complicated shapes with high precision and handle any conductive material with respect to its hardness, it has become one of the main techniques for producing miniature elements and parts that have a sub-micrometer size [6]. Lately, micro-EDM has been widely utilized in the field of dies, molds, nozzles, complex 3D structures and making holes with a high aspect ratio [7]. Due to its contactless interaction between the device and the workpiece, any conductive material can be machined by micro-EDM.

Titanium and its composites are utilized in different industries such as aviation, automotive and biomedical manufacturing because of its outstanding physical and mechanical characteristic, excellent corrosion tolerance and reduced elastic modulus [8,9]. Lack of mechanical behavior, reactivity to metal fabrication, cutting force constraint, splitting and abrupt metal cutting fatigue are all limitations in the traditional machining of Ti-6Al-4V [10]. Machining fast cooling holes in a Titanium alloy for aviation rotor blades has been one of the production problems and micro-EDM can be used successfully to drill such hole in Titanium alloys [11].

Different types of power generators such as resistance-capacitance (RC) circuit, bipolar junction transistor (BJT) circuit, MOSFET transistor circuit and hybrid circuit are used for spark ignition in the micro-EDM process [12]. The RC power generator can discharge a limited amount of energy by periodical charging and discharging of a capacitor, which is quite adequate for micromachining [13]. Since the capacitor needs time to charge, the RC circuit provides a low discharge energy and therefore the machining speed decreases whereas BJT circuits provide the benefits of a programmable pulse, which improves the processing speed [14]. A MOSFET transistor circuit generates a high peak current with high density and has a smaller pulse duration that provides fine discharge cavities, which leads to a significant material removal [15]. However, different types of pulse shape are generated by different power generator circuits and they influence the performance of the machining process differently. Rectangular current pulses have been widely used for this purpose.

If there is a need for excellent machining using micro-EDM, it is far vital to choose the machine parameters exactly for a conservative machining activity. Kobayashi and Oizumi found that, discharge current plays an important role in machining by influencing the output parameters such as tool wear and machining rate. Subsequently, it was observed that a specific pulse pit relies upon the discharge cutting edge pulse shape and the ideal pattern is distinct relying on the machining circumstances [16]. Ishikawa et al investigated different kinds of pulse shape such as rectangular, ramp up and ramp down. They state

that the evacuation efficiency of the ramp down pulse shape is better than that of other pulse shapes. Additionally, the quantity of debris generated depends on the pulse shape used [17]. Shinohara et al. investigated the same pulses as continuous pulse discharges and studied the impact of the difference in the machining charge among the three different pulse form become identical. The evaluation used to be carried out as it had been below a limited machining circumstance and the influence of the machining performance on the assurance of the pulse form exhibiting the most increases machining price has now not been defined at this factor [18]. Li et al. introduced a current wave shaping generator circuit for different waveforms such as rectangular and triangular pulse. It was found that the surface roughness was good in triangular due to a smaller pulse width whereas the processing speed and cutting performance of a rectangular waveform was good due to large discharge energy [19].

The literature review above shows that few studies are done on EDM of Titanium alloys using a regular pulse shape and there are no clear reports on different types of pulse shapes such as Sawtooth and its effect on the output. Hence, the present study focuses on micro-EDM of the Titanium alloys using Sawtooth pulse and the effect of various controlling parameters on the output. Statistical relationships are developed among various parameters and responses such as Material Removal Rate (MRR) and Overcut (OC) are analyzed. Further the parameters were optimized using Response Surface Methodology (RSM) to maximize MRR and minimize OC.

3. EXPERIMENT DETAILS

3.1 Machine tool

Titanium is widely utilized by various industries due to its outstanding features such as high robustness, sturdiness, and light weight. Titanium is categorized in four classes: unmixed Titanium, α structure, β structure and α-β structure. The different classes of Titanium are used for various applications. From these four, α-β structure is the most commonly used Titanium alloy, which is also called grade 5 Titanium alloy (Ti-6Al-4V). The chemical composition and mechanical properties of a Titanium alloy are shown in Tables 1 and 2.

A rectangular sheet of Ti-6Al-4V (50 mm x 35mm x 0.5 mm) was selected as the workpiece for the experiment. A piece of cylindrical copper wire (300 µm) was used as the tool material because of copper's remarkable thermal and mechanical properties. For the micro-EDM investigation, a micro-EDM setup was prepared for drilling a micro hole in the sheet (Figure 1). For a high precision micro machining process, we used three-axis programmed multi-measure machining on the alloy using deionized water as a dielectric fluid. This machine was powered by a MOSFET transistor circuit with a positional precision of 0.1 mm and Sawtooth current pulse. The following formulae have been used to calculate MRR and OC.

$$\mathrm{MRR} = \frac{\text{Weight of the workpiece before machining} - \text{weight of the workpiece after machining}}{\text{Time of machining process}}$$

$$OC = \frac{\text{Observed diameter of the machine electrode hole} - \text{Existing diameter of the electrode}}{2}$$

Table 1. Chemical composition of a Titanium alloy (Ti-6Al-4V)

Material	Titanium (Ti)	Aluminum (Al)	Vanadium (V)	Iron (Fe)
Wt%	89.62	6	4.02	0.22

Table 2. Mechanical properties of a Titanium alloy (Ti-6Al-4V)

Density	Tensile strength	Melting point	Thermal conductivity	Hardness
5.02g/cm^3	875MPa	1660 ^{0}c	6.7W/mK	3680MPa

Figure 1. Micro-EDM setup

3.2 Selection of input and output parameters

Experiments were conducted according to Face centered composite with three parameters and three levels. The parameters considered were current, T_{ON}, and T_{OFF} which directly affect the MRR and OC. Process parameters and their levels are shown in Table 3.

Table 3. Input parameters with its levels

Parameter	Level 1	Level 2	Level 3
Current (A)	5	7	9
T_{ON} (µs)	50	70	90
T_{OFF} (µs)	20	40	60

Micro-EDM was carried out at the constant time interval of three minutes and the workpiece was measured using a weighing machining with the accuracy of 0.001 gm (CY-360) before and after micro-EDM. To assess the overcut, the difference between the diameter of the machined hole and that of the copper wire were analyzed using SEM (JSM-6610LV Joel, Japan). Further, the machined specimens were examined to observe the surface morphology of the micro-EDM process using SEM.

4. RESULTS AND DISCUSSION

4.1 Response Surface Methodology

The correlations between a number of input variables and one or more output response variables are provided by RSM. In the current study, RSM is utilized to find the correlation between the input parameters furthermore the various responses, like MRR and OC. Statistical design became advanced to access the version among the effect (A), and method variables w_1, w_2,w_3,…….w_n and their correlations are given by the following equations:

$A=f(w_1, w_2, w_3…..w_n)$ (1)

Where A is the effect attribute

W_n is the method variables

In this study, three data variables have been used, current, T_{ON} and T_{OFF} and their effect on MRR and OC was analyzed.

The polynomial interaction effect were evaluated and is given in equation (2)

$$A_u=\beta_0+\sum_{i=1}^{k}\beta_i w_i+\sum_{i=1}^{k}\beta_{ii}w_i^2+\sum_{j>1}^{k}\beta_{ij}w_i w_j \quad (2)$$

Where A_u, predicted variable; w_n, control variables; β, regression coefficient; k, number input process.

The degree of computability of the impact by the modification of input factors on the output boundaries is numerically related with the ease of conditions refined from RSM. The observed current, T_{ON}, T_{OFF} are the highest considerable factors for the output estimation of MRR and OC. For 3x3 factors and levels, 20 different experimental levels were formed in RSM. Experiments were performed according to FCC and the results were analyzed using Minitab software. The outcomes of the experiment on Ti-6Al-4V using the current micro-EDM setup are presented in Table 4.

Table 4. Experimental results for MRR and OC

S. No	Current (A)	Pulse on time T_{ON} (µs)	Pulse off time T_{OFF} (µs)	MRR (mg/min)	OC (µm/min)
1	5	50	20	0.0240	50.23
2	9	50	20	0.0249	52.5
3	5	90	20	0.0269	54.2
4	9	90	20	0.0281	58
5	5	50	60	0.0241	51
6	9	50	60	0.0245	55.14
7	5	90	60	0.0274	56
8	9	90	60	0.0276	58
9	5	70	40	0.0263	53

10	9	70	40	0.0264	55.2
11	7	50	40	0.0249	54
12	7	90	40	0.0277	57
13	7	70	20	0.0265	56
14	7	70	60	0.0259	55
15	7	70	40	0.0265	56.1
16	7	70	40	0.0264	56.15
17	7	70	40	0.0263	55.16
18	7	70	40	0.0265	54.1
19	7	70	40	0.0261	55.31
20	7	70	40	0.0264	55.5

4.2 Statistical models for all responses

Table 5. Analysis of variance for Material removal rate

Source	DF	Adj SS	Adj MS	F-Value	P-Value
Model	9	0.000025	0.000003	63.45	0.000
Linear	3	0.000024	0.000008	182.51	0.000
Current	1	0.000001	0.000001	17.68	0.002
T_{ON}	1	0.000023	0.000023	528.01	0.000
T_{OFF}	1	0.000000	0.000000	1.83	0.206
Square	3	0.000001	0.000000	5.65	0.016
Current*Current	1	0.000000	0.000000	0.42	0.534
T_{ON} * T_{ON}	1	0.000000	0.000000	1.08	0.324
T_{OFF} * T_{OFF}	1	0.000000	0.000000	3.33	0.098
2-Way Interaction	3	0.000000	0.000000	2.21	0.150
Current* T_{ON}	1	0.000000	0.000000	0.03	0.870
Current* T_{OFF}	1	0.000000	0.000000	6.34	0.030
T_{ON} * T_{OFF}	1	0.000000	0.000000	0.25	0.625
Error	10	0.000000	0.000000		
Lack-of-Fit	5	0.000000	0.000000	2.91	0.133
Pure Error	5	0.000000	0.000000		
Total	19	0.000026			

Based on the equation (2), a statistical equations were developed for MRR and OC as given as below.

MRR=0.01580 + 0.000592 Current + 0.000117 T_{ON} + 0.000068 T_{OFF} - 0.000020 Current*Current- 0.000000 T_{ON} * T_{ON} - 0.000001 T_{OFF} * T_{OFF} + 0.000000 Current* T_{ON} - 0.000005 Current* T_{OFF} + 0.000000 T_{ON} * T_{OFF}

S= 0.0002106, R^2,=98.28% R^2(adj)=96.73%, and R^2(pred)=87.79%

The results of Material removal rate is calculated and listed in Table 5.

The effects of input parameters such as T_{ON}, T_{OFF} and current on the output of OC can be given as follows:

OC = 26.77 + 5.28 Current + 0.088 T_{ON} + 0.028 T_{OFF} - 0.316 Current*Current + 0.00034 T_{ON} * T_{ON} + 0.00034 T_{OFF} * T_{OFF} - 0.00191 Current* T_{ON} + 0.00022 Current* T_{OFF} - 0.000503 T_{ON} * T_{OFF}

S = 0.776541, R^2 = 95.92%, R^2(adj) = 92.24%, and R^2 (pred) = 87.97%

Table 6. Analysis of Variance for OC

Source	DF	Adj SS	Adj MS	F-Value	P-Value
T_{ON}	9	70.5026	7.8336	10.28	0.001
T_{OFF}	3	63.8681	21.2894	27.93	0.000
Square	1	20.7648	20.7648	27.24	0.000
Current*Current	1	41.3309	41.3309	54.21	0.000
T_{ON} * T_{ON}	1	1.7724	1.7724	2.32	0.158
T_{OFF} * T_{OFF}	3	6.2634	2.0878	2.74	0.099
2-Way Interaction	1	4.4069	4.4069	5.78	0.037
Current* T_{ON}	1	0.0494	0.0494	0.06	0.804
Current* T_{OFF}	1	0.0494	0.0494	0.06	0.804
T_{ON} * T_{OFF}	3	0.3711	0.1237	0.16	0.919
Error	1	0.0465	0.0465	0.06	0.810
Lack-of-Fit	1	0.0006	0.0006	0.00	0.978
Pure Error	1	0.3240	0.3240	0.43	0.529
Total	10	7.6237	0.7624		
T_{ON}	5	4.8066	0.9613	1.71	0.286
T_{OFF}	5	2.8171	0.5634		
Square	19	78.1263			

Statistical analysis of the specific characteristics on MRR and OC was investigated using ANOVA (Tables 5 and 6). The estimated F-values for the calculated quadratic are 63.45 and 10.28, respectively, implying that the value of OC and MRR is important for the specified quadratic representation. That the feasibility (p-values) 0.0500 is much less than the F-value shows that the version time period is significant. Probabilities which might be more than 0.1000 results in non-significance phrases. In phrases of natural error, the insignificant F-value for the Lack of Fit is 2.91 for MRR while for the overcut it is 1.71. The F-value of the Lack of Fit for MRR and OC, appropriately, has the likelihood of 98.28% and 95.92% that is only caused by noise. The R^2 value of the determination coefficient represents the model's compatibility, which ranges from 0 to 1. Tables 5 and 6 show that applied current, T_{ON}, and T_{OFF} have substantial effects on both MRR and OC. Hence, it is observed to be well-being fit of model data values. Figure 2 shows the regular contingency design on the effect of MRR when analyzed. It can be observed that residuals are spread around in an orderly fashion, which shows a great correlation among the experimental and anticipated values. It also can be inferred that the faults are normally distributed. The regular contingency design of residues for OC is shown in Figure 3. That majority of the residuals lie on a straight line indicates that the faults are regularly distributed. It demonstrates that the regression model fits the observed values fairly well. Non-significant terms are

removed from the model during its development. A Pareto chart has been drawn to check the most extensive variable on the reaction that is shown in Figures 4 and 5. Linear terms, squared terms, interaction effects, and a reference line are all part of it. Figure 4 shows that T_{ON} has more effect on the result boundary than other input parameters. The crimson line represents the reference line, which is determined at the recommended overall performance level of 95%. As per the Pareto graph in Figure 4, T_{ON}, T_{OFF} and the interaction influence of T_{ON} and current are the most significant variables for MRR. From the Pareto graph in Figure 5, T_{ON}, T_{OFF}, current and interaction of T_{ON} and T_{OFF} can be seen as the most impactful factors for OC and that T_{ON} has more influence on the output parameters than current and T_{OFF}.

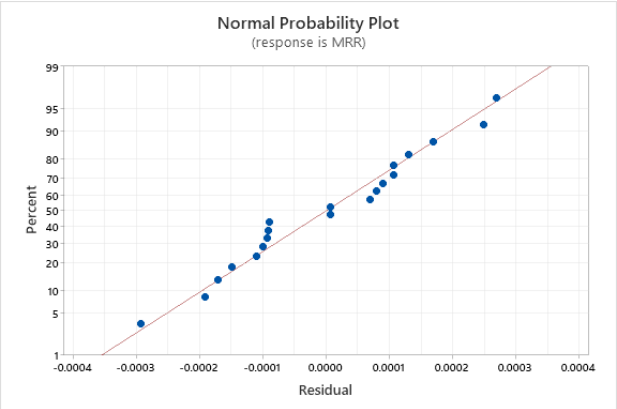

Figure 2. Normal probability plot for MRR

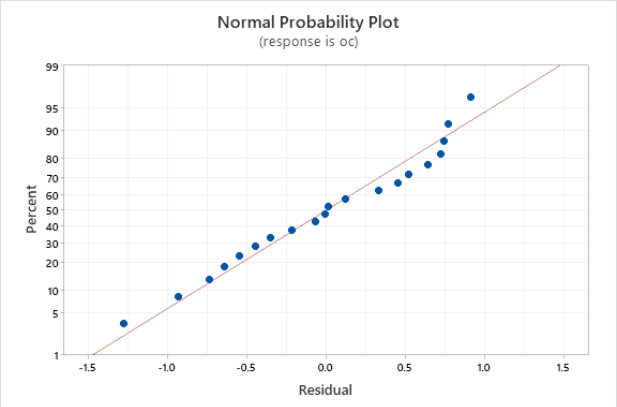

Figure 3. Normal probability plot for OC

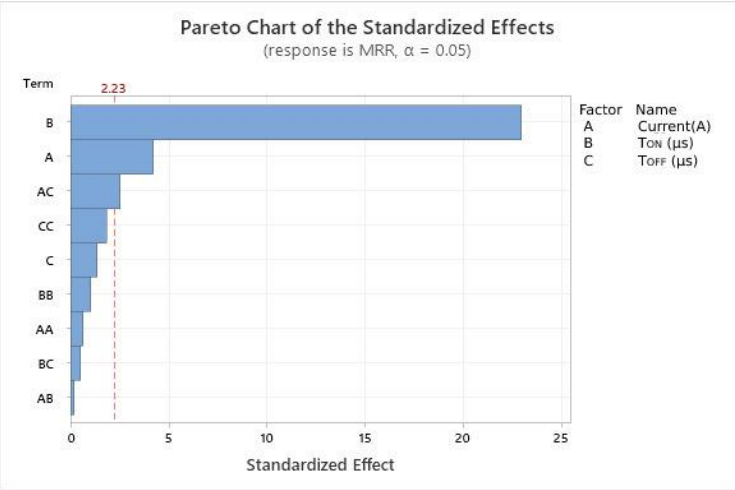

Figure 4. Pareto optimal front for MRR

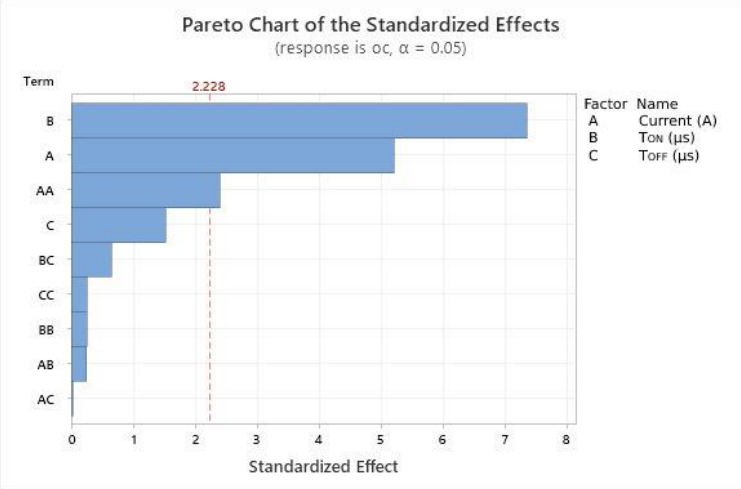

Figure 5. Pareto optimal front for OC

4.3 Impact of control variables on material removal rate

Figure 6 shows the impact of current on MRR and that as the current increases from 5 to 7A, MRR too increases linearly. This is because at lower current values, the amount of energy generated in the gap is small, which is not adequate to melt and vaporize the workpiece surface rapidly. With a further increase in the current from 7A to 9A, the energy becomes more intense and causes melting and vaporization of the workpiece surface. This generates more debris during machining and impedes the energy supplied to the workpiece, so there is no further improvement in the MRR [20]. More high current generates more thermal energy in the gap, causing more frequent stern cracking of the dielectric which leads to the formation of a molten pool that overheats to form bigger craters (Figure 7) [21].

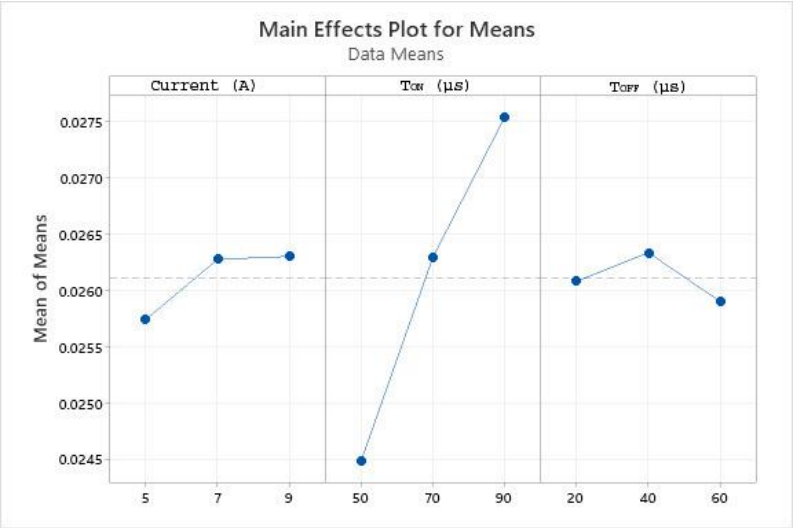

Figure 6. Effect of control factors plots on MRR

Figure 6 reveals that as T_{ON} raises from 50µs to 90µs, the spark discharge prolongs and generates higher discharge energy that increases the MRR. At T_{ON} of 50µs, the amount of the material removed from the workpiece is minimum when the discharge within the machining hole becomes less intense. At the T_{ON} of 90µs, the spark energy might be excessive and generate enormous heat in the machining area. Even more heat removes a sizeable quantity of material from the workpiece [22].

In addition, during a higher $T_{ON,}$ more material melts and gets redeposited on the workpiece surface, which releases the gas that gets entrapped during the machining and forms voids and pockmarks as illustrated in Figure 8. From the Figure 6, the T_{OFF} increases from 20µs to 40µs, surged and decreases from 40µs to 60µs. At a lower T_{OFF} of 20µs, the base current provided to the cathode and the dielectric fluid is high, which is high enough to melt the workpiece surface and the anode, which subsequently increases the MRR [23]. MRR diminishes as the T_{OFF} value changes from 40µs to 60µs. This means that with a higher $T_{OFF,}$ no energy is supplied to the workpiece for a longer time. The debris formed during micro-EDM processes were evacuated efficiently [24].

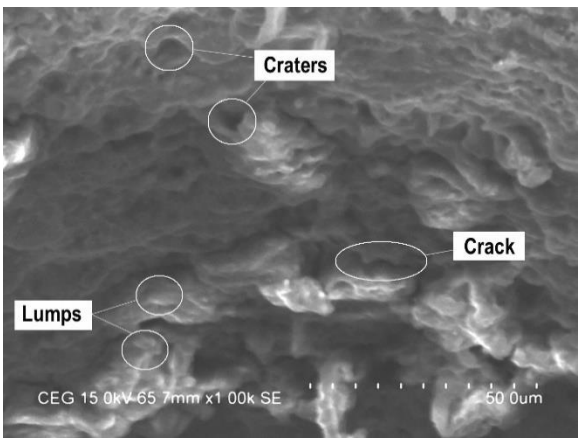

Figure 7. SEM image at a peak current of 9A

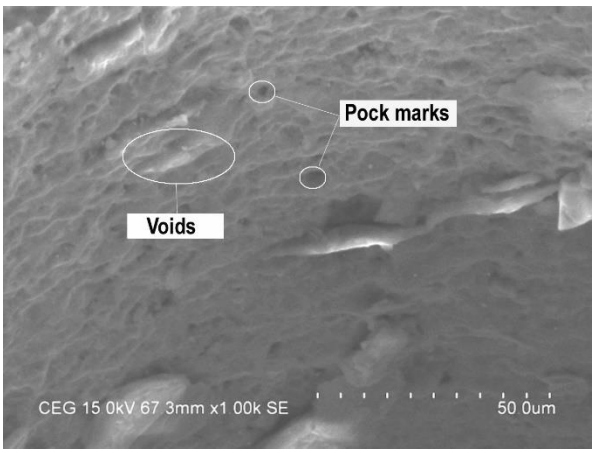

Figure 8. SEM image at a higher T_{ON} of 90µs

4.4. Impact of control variable on overcut

The main effect plots of the current, T_{ON}, T_{OFF} on element characterization are shown in Figure 9. It was found that OC increases with a rise in the current from 5A to 7A. It was also noticed that when the peak current increases from 5A to 7A, the discharge spark also increases, causing the breakdown of debris into smaller particles. On a further increase of the current from 7A to 9A, the resultant debris cannot be easily evacuated through the narrow path and it abrades the entrance of the machined hole causing a higher OC as shown in Figure 10.

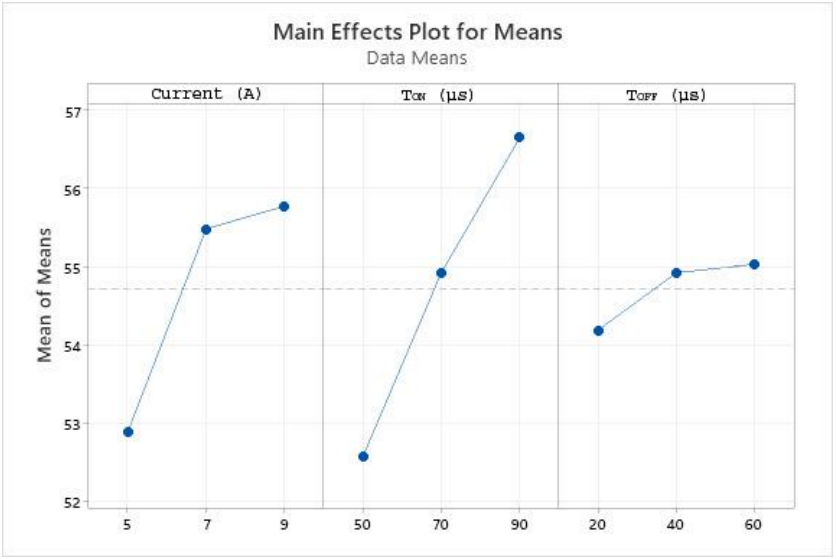

Figure 9. Effects of control factors plots on OC

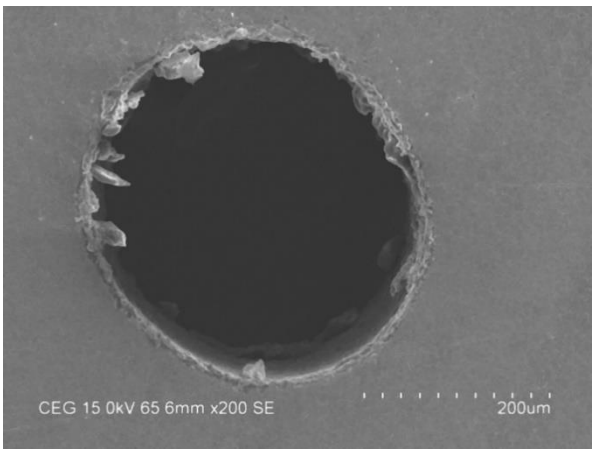

Figure 10. SEM microgap of machined hole at a peak current of 9A

The significant effect of Sawtooth T_{ON} on OC is shown in Figure 9 where T_{ON} increases from 50µs to 90µs. For a smaller pulse of 50µs, less power is tranmitted to the Titanium alloy, which results in a small material removal as well as less OC with a good dimensional accuracy (Figure 11) [25]. When T_{ON} reaches 90µs, the OC increases. This is due to the production of stray current flux at the machining region and it leads to an increase in the OC as can be seen in Figure 12 [26].

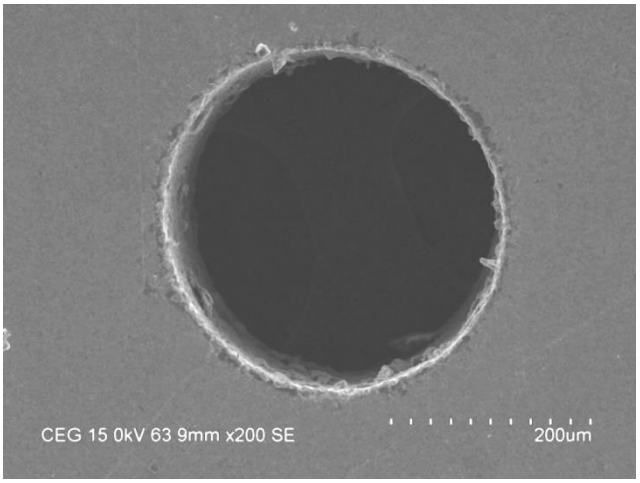

Figure 11. SEM micrograph of machined hole of T_{ON} (50µs)

The correlation between T_{OFF} and overcut is depicted in Figure 9. It was observed that when T_{OFF} increases from 20µs to 40µs, the plasma channel spawned was smaller and released a small amount of spark energy to hit the surface, which reduces the dimensions of the crater on the surface, leading to a lower OC. However, a higher pulse-off time (40µs to 60µs) means that the supply of spark energy is stopped longer during machining, hence no conductive path is created in the Inter Electrode Gap (IEG), results in evacuating the debris from the IEG by flushing of dielectric leads to decline in the OC.

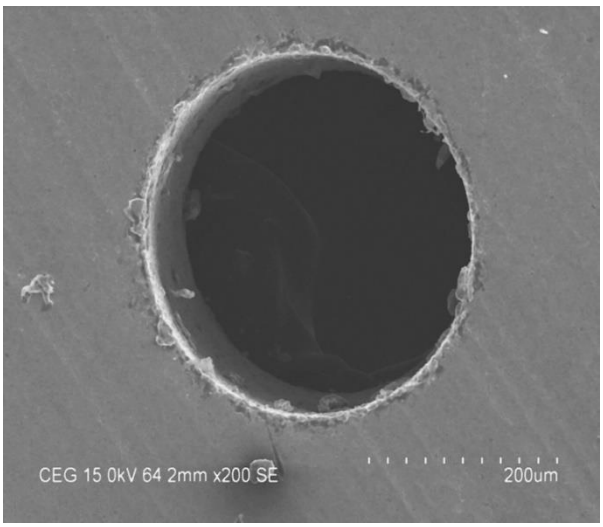

Figure 12. SEM micrograph of machined hole of T_{ON} (90µs)

5. CONCLUSIONS

The current study investigated micro-EDM performance on a Titanium alloy and variables such as MRR and OC were analyzed and statistical models were developed. The results of ANOVA show that the developed models are adequate. Graphs for several micro-EDM parameters are also presented for the output performance. The Figures show that MRR improves as the pulse-on time and current increases. This could be described by the fact that a higher quantity of thermal intensity is released and maintained for an extended time period, enabling the workpiece surface to melt and vaporize faster. MRR, on the other hand, drops when the pulse-off time is higher. This is due to fact that when the supply of spark energy is cut off for a prolonged time, no conductive route is generated in the IEG, leading to a a lower MRR.

OC increases when the pulse-on time and applied current increases. A larger overcut is caused by bigger values of the pulse-on time and applied current, which generate a high temperature as positive ions in IEG strike the electrode surface with a high spark energy. Increased pulse-off time, on the other hand, clears the debris by flushing the dielectric fluid out of the system, that results in a decrease in the OC.

References

1. B.Z. Balázs, N. Geier, M. Takács and J.P. Davim, *The International Journal of Advanced Manufacturing Technology*, 112 (2021) 655.
2. J. E. Abu Qudeiri, A. Zaiout, A-H. I. Mourad, M. H. Abidi and A. Elkaseer, *Applied sciences*, 10 (2020) 2082.
3. S.N. Grigoriev, P.M. Pivkin, M.P. Kozochkin, M.A. Volosova, A. A. Okunkova, A.N. Porvatov, A. A. Zelensky and A. B. Nadykto, *Metals*, 11(2021) 1865.
4. A.Y. Joshi and A.Y. Joshi, *Heliyon*, 5 (2019) e02963.

5. P.K. Shrivastava, A.K. Dubey, *Institution of Mechanical Engineering Manufacture*, 228 (2013) 799.
6. A. Bilal, M.P. Jahan, D. Talamona and A. Perveen, *Micromachines*, 10 (2019) 10.
7. J.E. Abu Qudeiri, A. Saleh, A. Ziout, A-H.I. Mourad, M.H. Abidi and A. Elkasee, *Materials*, 12 (2019) 907.
8. P. Pesode and S. Barve, *Materialstoday proceedings*, 46 (2021) 594.
9. Y. Li, C. Yang, H. Zhao, S. Qu, X. Li and Y. Li, *Materials (Basel)*, 7 (2014) 1709.
10. M.D. Hayat, H. Singh, Z. He and P. Cao, *Applied Science and Manufacturing*, 121 (2019) 418.
11. A. Pramanik and G. Littlefair, *Machining Science and Technology*, 19 (2015) 1.
12. H-G. Cheong, Y-S. Kim, C-N. Chu, *Procedia CIRP*, 68 (2018) 631.
13. X Chu, W. Feng, C. Wang and Y. Hong, *International Journal of Advance Manufacturing Technology*, 89 (2017) 317.
14. Q. Liu, Q. Zhang, M. Zhang and F. Yang, *Micromachines*, 11 (2020) 55.
15. F. Han, C. Li, D Yu and X. Zhou, *International Journal of Advance Manufacturing Technology*, 33 (2007) 474.
16. K. Kobayashi and T. Oizumi, *Journal of The Japan Society of Electrical Machining Engineers*, 8 (1975) 20.
17. A. Ishikawa, M. Kunieda. *Journal of the Japan Society for Precision Engineering*, 8 (2019) 717.
18. T. Sultan, A.Kumar and R.D. Gupta, *International Journal of Manufacturing Engineering*, 2014
19. C.J. Li, J.J Ding, S.Q. Yang, Y.S. Fang, Q.C. Kong, *The International Journal of Advanced Manufacturing Technology*, 87 (2016) 371.
20. B. Choudhuri, R. Sen, S. K. Ghosh and S.C. Saha *Institution of Mechinal Engineers*,231 (2015) 1760.
21. A. Jamwal, A. Aggarwal, N. Gautam, A. Devarapalli, *International Research Journal of Engineering and Technology*, 5 (2018) 433.
22. P. K. Patowari, P. Saha and P. K. Mishra, *International Journal of Advance Manufacturing Technology*, 54 (2011) 593.
23. C. Balasubramaniyan, K. Rajkumar and S. Santhosh, *Material Manufacturing Process*, 36 (2021) 1161.
24. K. Yadav, P. Kumar and A. Dvivedi, *Material Manufacturing Process.* 34 (2019) 1832.
25. V. Muthukumara, N. Rajesha, R. Venkatasamya, A. Sureshbabub and N. Senthilkumar, *Procedia Material Science*, 6 (2014) 1674.
26. N. Ahmed, K. Ishfaq, M. Rafaqat, S. Pervaiz, S. Anwar and B. Salah. *Material Manufacturing Process*, 34 (2019) 769.

© 2022 The Authors. Published by ESG (www.electrochemsci.org). This article is an open access article distributed under the terms and conditions of the Creative Commons Attribution license (http://creativecommons. org/licenses/by/4. 0/).